Type-II Kinase Inhibitor Docking, Screening, and Profiling Using Modified Structures of Active Kinase States

Irina Kufareva[†] and Ruben Abagyan*[,†,‡]

The Scripps Research Institute, La Jolla, CA, and Molsoft, LLC, La Jolla, CA

Received August 14, 2008

Type-II kinase inhibitors represent a class of chemicals that trap their target kinases in an inactive, so-called DFG-out state, occupying a hydrophobic pocket adjacent to the ATP binding site. These compounds are often more specific than those that target active DFG-in kinase conformations. Unfortunately, the discovery of novel type-II scaffolds presents a considerable challenge, partially because the lack of compatible kinase structures makes structure-based methods inapplicable. We present a computational protocol for converting multiple available DFG-in structures of various kinases (~70% of mammalian structural kinome) into accurate and specific models of their type-II bound state. The models, described as deletion-of-loop Asp-Phe-Gly-in (DOLPHIN) kinase models, demonstrate exceptional performance in various inhibitor discovery applications, including compound pose prediction, screening, and in silico activity profiling. Given the abundance of the DFG-in structures, the presented approach opens possibilities for kinome-wide discovery of specific molecules targeting inactive kinase states.

Introduction

Protein kinases have long been recognized as important drug targets.[1] Several dozen small molecule kinase inhibitors are either approved or studied for various human diseases including cancer, cardiovascular disorders, and inflammation.[2,3]

Functional states of a typical protein kinase can be characterized by the position of a conserved DFG[a] (or, rarely, D[LWY]G) motif in its activation loop. The absolute majority of inhibitors targets the ATP site of the kinase in its active DFG-in state. In contrast, the so-called type-II inhibitors (e.g., imatinib and sorafenib) induce a distinct DFG-out conformation and occupy an additional hydrophobic pocket created by this rearrangement[4−8] (Figure 1a). These inhibitors possess several advantages over ATP-site compounds, including improved kinase selectivity and slower off-rates.[9]

The phenomenon of type-II inhibition was initially thought to be specific to only a few protein kinases. A small residue at the so-called gatekeeper position in the kinase hinge region was considered to be a prerequisite for type-II inhibition. That view is challenged by recent advances in targeting kinases with medium-size gatekeepers, such as TIE and MET.[10−12] Type-II inhibitor discovery for a wider range of kinases is therefore a topic of great interest and importance.

Unfortunately, the de novo identification of type-II inhibitors presents a considerable challenge. They are often overlooked in traditional enzymatic assays and high-throughput screening (HTS) because of low affinity for active phosphorylated kinases. To overcome this obstacle, several phosphorylation state-independent binding assays have been developed, some involving competition binding to immobilized probes [13−16] and others based on temperature-dependent unfolding of the protein.[17−19] These assays, however, address the problem only partially because they are not as cost effective as biochemical assays and are hard to apply in a high-throughput fashion. Not surprisingly, most known type-II inhibitors to date have been developed via QSAR-guided modifications of ATP-site ligands rather than directly from HTS.

The QSAR strategies were generalized by Liu and Gray[20] and Okram et al.,[21] who presented a universal chemical modification protocol that converts known ATP-site inhibitors into their type-II counterparts. This revolutionary work demonstrated that type-II inhibition is a relatively common phenomenon for which general methods can be successfully developed and applied. Their approach, however, was restricted to only a small fraction of chemical space and, being completely chemistry-based, yielded compounds with unpredictable kinase specificity.

Structure-based computational methods, including virtual ligand screening (VLS), have the potential to both dramatically widen the chemical space and reduce the number of candidates for experimental validation. VLS techniques were found to be successful in a wide variety of applications (e.g., refs 22−24), especially when combined with improved scoring functions.[25,26] However, the lack of relevant kinase structures limits the applicability of these techniques to type-II inhibitor discovery. The absolute majority of the existing kinase structures is type-II incompatible. That includes the DFG-in structures, representing ~70% of the mammalian structural kinome, the intermediate (~22%), and even the apo-DFG-out (~3%) structures. Reliable methods for modeling the DFG-in/DFG-out transition have not been reported to date.

Here we propose a new approach to structure-based type-II inhibitor discovery and evaluation. We designed a general deterministic modeling protocol for converting the abundant DFG-in structures of various kinases into accurate and specific models of their type-II bound state, the so-called DOLPHIN (deletion-of-loop Phe-in) kinase models. The models were

* Corresponding author. Address: Department of Molecular Biology, TPC28, The Scripps Research Institute, 10550 North Torrey Pines Road, La Jolla, CA 92037. E-mail: abagyan@scripps.edu. Tel: 00 1 (858) 784 8595. Fax: 00 1 (858) 784 8299.

† The Scripps Research Institute.

‡ Molsoft, LLC.

[a] Abbreviations: AUC, area under curve; DOLPHIN: deletion-of-loop Asp-Phe-Gly-in models; DFG, conserved Asp-Phe-Gly motif; ICM, internal coordinate mechanics; HTS, high-throughput screening; MRC, multiple receptor conformations; QSAR, quantitative structure activity relationship; rmsd, root mean square deviation; ROC, receiver operating characteristic; VLS, virtual ligand screening.

10.1021/jm8010299 CCC: $40.75
Published on Web 11/18/2008

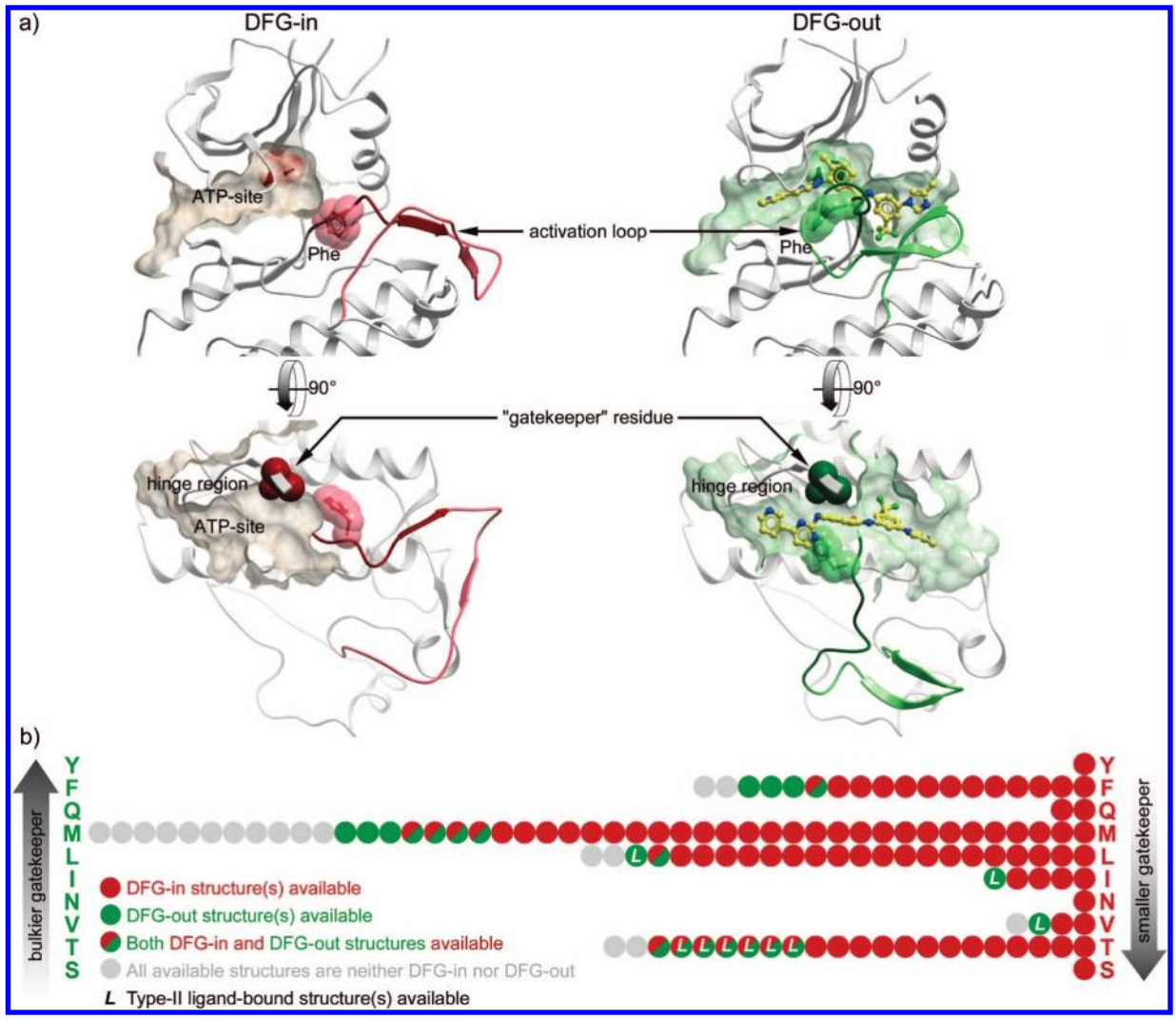

Figure 1. (a) Type-II inhibitors induce, stabilize, and exploit a distinct DFG-out conformation of the target kinases. (b) Conformational statistics of mammalian structural kinome (based on PDB release of June 2008).

validated on a comprehensive kinase−ligand benchmark and demonstrated exceptional performance in all three types of structure-based inhibitor discovery applications: (i) ligand docking (binding pose prediction), (ii) ligand screening (recognition of active type-II compounds in a large data set), and (iii) ligand activity profiling (evaluation of the relative ligand affinities to different kinases). Given the extensive representation of the DFG-in conformations in structural kinome, this approach creates new possibilities for the discovery of novel type-II inhibitors for a wide range of kinases.

Results

DFG-In Conformations are Predominant in the Structural Kinome. The June 2008 release of the Protein Data Bank[27] contained 1216 structures of 122 mammalian protein kinase domains. Conformational analysis of this set showed that 95 kinases were represented at least once in the DFG-in state (840 structures) (Figure 1b). The set of type-II-compatible structures, on the contrary, was limited to only nine kinases (ABL1, LCK, MET, KIT, SRC, BRAF1, VGFR2, TIE2, and MK14) that have already been cocrystallized with type-II inhibitors (69 structures). Neither 268 structures of intermediate conformations nor even 39 apo-DFG-out structures represented reasonable models of type-II-bound states.

Conservation of Structural Features of Type-II-Bound Conformations in the DFG-In State Suggests DOLPHIN Transformation. DFG-in/DFG-out transition is a dramatic conformational change induced by type-II kinase inhibitors and their characterizing feature. We observed, however, that except for the DFG-out state, determinants of type-II ligand binding are preserved in most DFG-in structures. These determinants include (i) the presence of the conserved lysine−glutamate salt bridge and (ii) sufficient pocket width (the distance between the carboxyl group of the conserved αC-helix glutamate and the backbone amide nitrogen of the DFG-motif aspartate).

With reasonable margins, both the conserved salt bridge and the sufficiently wide pocket (>4.3 Å) were observed in as many as 600 mammalian DFG-in structures (71%). Some representative counterexamples included PDB 1pkg (activated KIT kinase, pocket width of only 4.2 Å), 1fmk (SRC kinase, conserved glutamate points away from the active site), and chain B of PDB 1yom (SRC, conserved glutamate disordered). Fortunately, these cases were a minority.

Structural conservation of the two determinants of type-II inhibition suggested that DFG-motif excision might convert the DFG-in structures into accurate models of type-II-bound state of their respective kinases, which led to the development of the DOLPHIN protocol (Figure 2, Methods Section). To

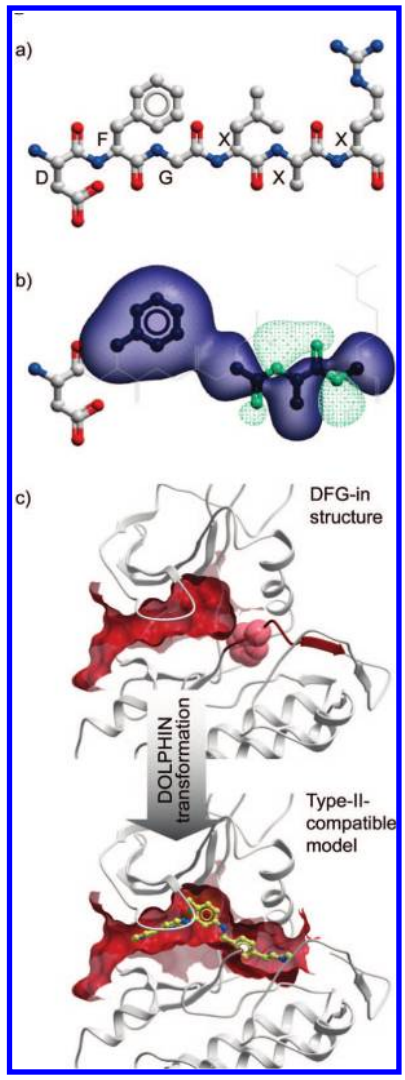

Figure 2. DOLPHIN transformation. (a) DFG Phe and the next four residues in the sequence are removed. (b) Attractive density is generated from selected removed atoms. The transparent blobs represent equipotent contours of the lipophilic (dark-blue) and polar (sea-green) parts of the density. (c) This computational surgery dramatically affects the ligand binding pocket shape and size, producing a type-II compatible model.

compensate for possible crystallographic errors and to enhance the model performance, we also introduced a weak nonspecific pharmacophore-like field in place of selected removed atoms.

Testing DOLPHIN Models in Single and Multiple Receptor Conformation Modes. The models were tested in docking, screening, and activity profiling of the known type-II inhibitors in two modes. In the so-called single receptor mode, the performance of each DOLPHIN was evaluated separately. In the multiple receptor conformations (MRC) mode, all available DOLPHINs of a single kinase were combined and each compound was represented by its best score in this ensemble.

The minority of DFG-in structures with narrow pocket, disrupted salt bridge, or both was expected to demonstrate inferior performance in the above applications. We nevertheless included these structures in the experiment for the sake of exhaustiveness and to evaluate the relative roles of the two structural features.

The models were tested on a comprehensive benchmark of publicly available DFG-in and type-II-bound kinase structures described in the Methods Section.

Docking to a Single Rigid DOLPHIN Model Correctly Predicts Type-II Ligand Binding Geometry in over 75% of the Cases. In the single receptor docking, the near-native ligand binding geometry scored first for 142 of 184 DOLPHIN ligand pairs (77%). In 153 cases (83%), it was found within three top-scoring ligand conformations (Table 1). The standard ligand heavy-atom rmsd cutoff of 2 Å was applied.

The docking performance of individual models significantly varied. For example, several models of the SRC kinase appeared to be incompatible with compound **1** (imatinib,[4] PDB Het ID STI, Figure 3) because of a disrupted salt bridge or other structural deviations. Interestingly, imatinib is an extremely weak binder to SRC kinase[28] (observable $K_d > 10\ \mu M$), which might be due to low representation of appropriate SRC conformations in solution. Correct ligand placement also presented a challenge for both narrow-pocket DOLPHINs of the KIT kinase (1pkgA,B). Importantly, the imatinib-resistant active site mutation, T315I, made 2v7aA and 2v7aB the lowest-performing structures of ABL1. In contrast with these examples, the most accurate models (e.g., 2g2iA, 2qohA,B and 1oz1A) reproduced the binding geometry of all benchmark compounds.

Despite a sufficiently wide pocket and intact salt bridge, chain C in the 2hz4 structure of ABL1 kinase appeared to be a difficult target. We explain it by very high (>100) B-factors of the pocket atoms in this chain signaling unstable crystal and leading to the unusual, type-II-incompatible rotameric state of Met290.

Among the ligands, the most difficult was compound **2** (an anilinoquinazoline type-II inhibitor of MK14,[29] PDB Het ID AQZ). In the cocrystal of the kinase with **2** (PDB 2bak), the DFG Phe169 is reoriented toward the hinge region and provides a stabilizing ligand interaction. The absence of this residue in DOLPHIN complicated the ligand positioning so that its hinge-region moiety correctly docked in only 2 of 6 cases. However, the part of the ligand occupying the hydrophobic selectivity pocket correctly docked in all cases with a partial rmsd below 1 Å.

Contribution of the Pharmacophore-like Field. As described above, a weak attractive field was introduced as a part of the DOLPHIN models in place of their removed DFG-motif atoms. Interestingly, most models were sufficiently accurate to achieve similar docking performance even in the absence of the field. Without it, the correct ligand binding geometry scored first in 112 of 184 cases (61%) and was within the top three poses in 141 cases (77%).

Multiple Receptor Conformation Mode Further Improves Pose Prediction. When only the best-scoring ligand poses were selected for kinases with multiple DFG-in structures, the correct binding geometry ranked first for as many as 21 of 23 kinase/ligand pairs (91%) (Figure 4). For the 22nd pair (MK14 and compound **2**), it ranked third, yielding to two poses with correctly docked hydrophobic pocket moiety. The only unsuccessful pair consisted of the narrow-pocket KIT ensemble and imatinib, with the near-native geometry ranking only ninth. For 18 of 23 kinase/ligand pairs, pose prediction was also successful in the absence of the pharmacophore-like field.

Refinement and rescoring of the top three ligand poses raised the success rate to 22 of 23 cases (95%), with the pair of MK14 and compound **2** included. The improvement was apparently due to the use of full-atom scoring procedure that is more sensitive to hydrogen bonding and therefore rewards ligand poses with optimal hinge-region contacts.

DOLPHIN Models Recognize Type-II Inhibitors of Their Respective Kinases in Virtual Screening. We further studied the ability of DOLPHIN models to distinguish the active

Table 1. Root Mean Square Deviation (rmsd) Values for Top-Scoring Docking Poses of Crystallographic Type-II Ligands in DOLPHIN Models of Their Respective Kinase Targets[f]

ABL1 DFG-in	406	7MP	GIN	KIN	PRC	STI
2f4jA	1.91	0.46	0.87	0.62	1.73	0.52
2g2iA	1.14	0.65	1.11	0.67	1.67	0.76
2g2iB	2.12 (2)	0.53	3.76 (2)	0.71	2.62 (5)	0.98
2gqgA[a]	2.09 (4)	0.83	2.06 (2)	0.98	12.62 (16)	1.69
2gqgB	1.85	1.90	0.85	0.89	2.06 (8)	1.75
2hz4A	0.92	1.98	0.99	0.84	12.72 (9)	6.65 (3)
2hz4B	1.37	1.03	0.85	0.62	1.92	1.55
2hz4C	7.44 (12)	1.70	11.66 (4)	12.35 (5)	14.99 (40)	11.11 (26)
2qohA	0.88	0.68	0.89	0.73	1.56	0.60
2qohB	1.09	0.97	1.23	0.64	1.58	0.81
2v7aA[b]	4.32 (44)	8.22 (10)	10.34 (61)	0.97	9.97 (47)	13.19 (51)
2v7aB[b]	13.19 (149)	9.36 (23)	10.49 (NS)	1.12	10.85 (48)	9.23 (62)
2z60A[b]	1.04	1.93	1.92	0.74	12.20 (3)	1.06

BRAF1 DFG-in	BAX
2fb8A	1.59
2fb8B	0.62

KIT DFG-in	STI
1pkgA[a]	4.11 (3)
1pkgB[a]	3.73 (3)

LCK DFG-in	1N8	242	9NH	STI
1qpcA	1.13	0.77	1.01	1.49
1qpdA	1.02	0.71	1.36	1.44
1qpeA	1.28	1.63	1.30	1.61
1qpjA	1.03	0.47	0.83	1.39
2of2A	1.21	0.76	1.41	1.55
2of4A	1.23	0.74	1.05	1.50
2ofuA	1.28	0.54	1.01	1.40
3lckA	1.43	0.76	2.06 (2)	1.41

SRC DFG-in	STI
1fmkA[c]	11.91 (NS)
1y57A	1.33
1yi6A	16.33 (3)
1yi6B[a]	2.80 (4)
1yomB[d]	5.18 (57)
2bdfA[a]	7.11 (2)
2bdfB[a]	7.02 (3)
2bdjA[a]	1.12
2hwoA[d]	13.77 (18)
2oiqB[a]	1.12

MK14 DFG-in	1PP	AQZ	B96	BMU	L09	L10	L11	LI2	LI3	WBT
1m7qA	0.62	3.16[e] (5)	0.77	1.07	1.58	0.45	1.03	0.73	1.40	0.68
1oukA	0.67	3.17[e] (4)	0.80	0.93	1.40	0.68	0.77	0.79	1.50	0.75
1ouyA	0.73	3.61[e] (15)	0.76	1.12	1.81	0.49	1.19	0.99	1.50	0.90
1oz1A	0.65	1.29	1.17	0.97	1.14	0.44	0.57	0.82	0.85	0.62
2okrA	0.75	1.49	4.36 (4)	1.08	10.99 (11)	0.67	1.32	1.35	1.43	1.30
2okrD	0.80	4.56[e] (NS)	4.30 (82)	1.27	1.85	0.68	1.45	1.57	1.56	1.46

[a] Narrow pocket. [b] T315I imatinib-resistant mutation. [c] Conserved salt bridge disrupted. [d] Conserved salt bridge disordered. [e] Part of the ligand occupying the hydrophobic selectivity pocket docked correctly with partial rmsd < 1A. [f] Table entries are in the format rmsd (rank first correct, if not 1); NS = not sampled. Correct poses ranking first are colored green, within top three yellow, otherwise grey. All compound chemical structures can be found in Figure S1 in the Supporting Information.

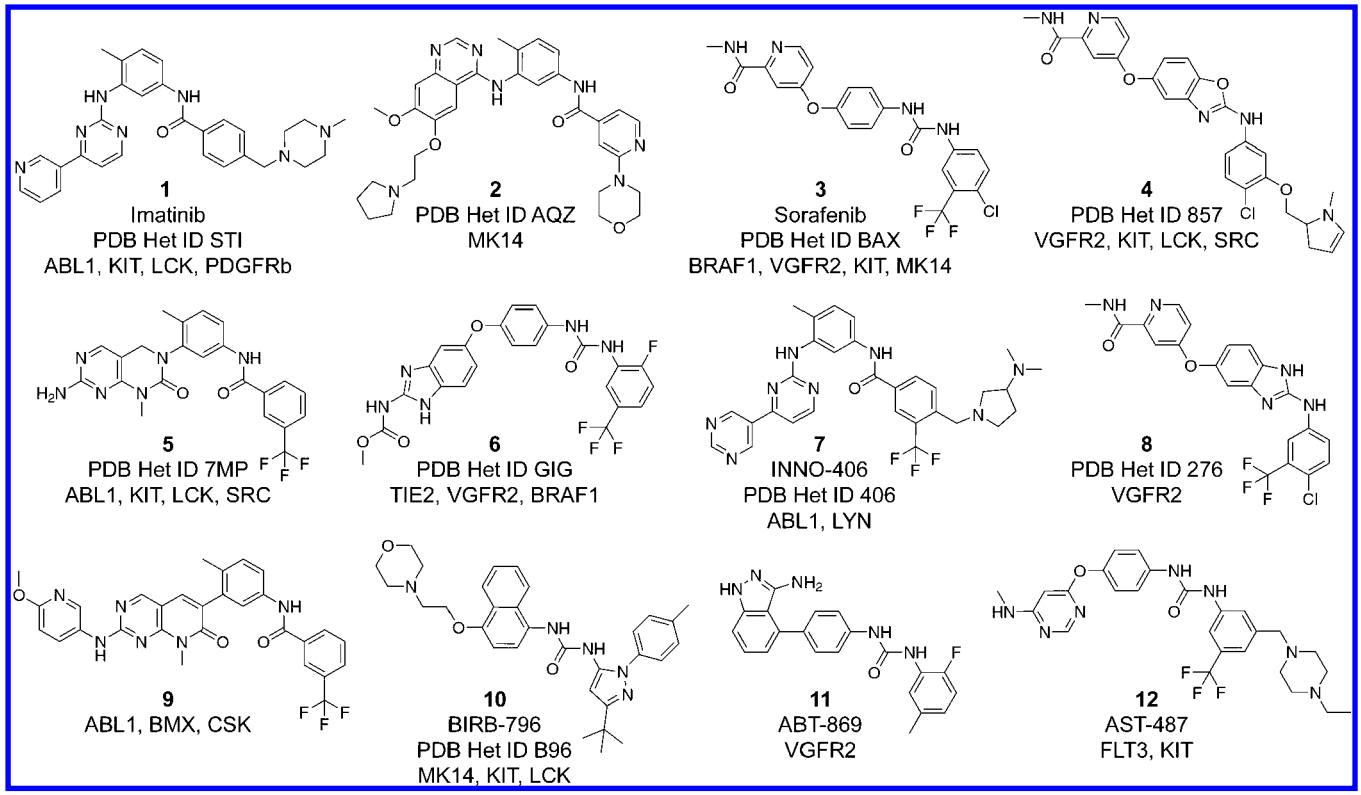

Figure 3. Chemical structures, names, and targets of type-II kinase inhibitors mentioned in the text.

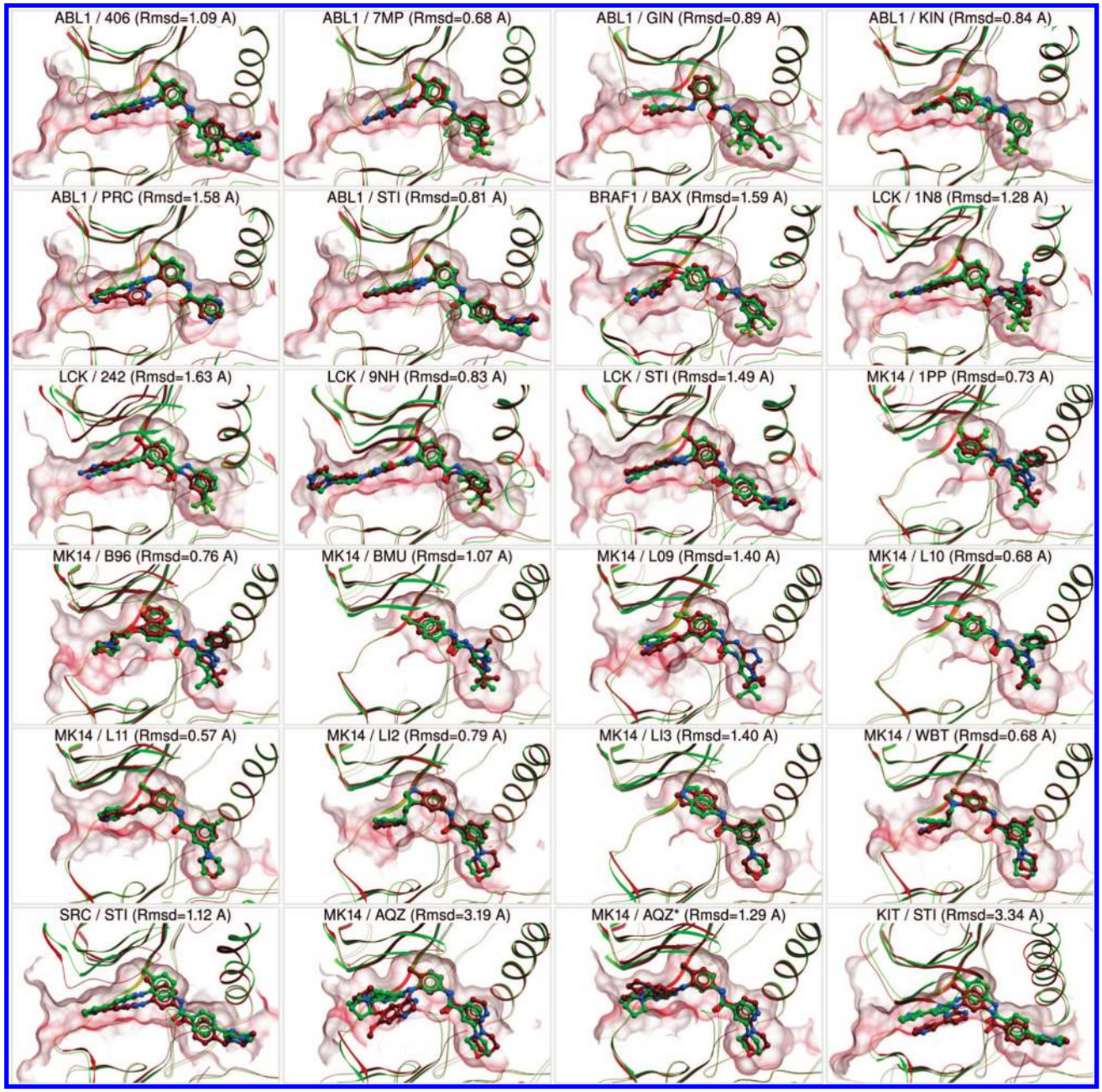

Figure 4. Comparison of the top-scoring poses of the crystallographic type-II ligands in DOLPHIN MRC ensembles of their target kinases (red) with the crystallographic complexes (green). *For MK14 and compound **2** (PDB Het AQZ), the correct pose was ranked first after refinement and full-atom scoring.

type-II inhibitors from other compounds in VLS. A data set of 391 crystallographic kinase ligands was used for this purpose, a fraction of active type-II inhibitors ranging from 0.7% for BRAF1 and SRC to 3.6% for MK14. Docking and scoring the data-set compounds in each DOLPHIN model produced an ordered hit list with the challenge of bringing the scarce active inhibitors to its top. The model screening performance was evaluated numerically as the area under the ROC curve, or AUC.

Virtual Ligand Screening with a Single DOLPHIN Model. As Table 2 illustrates, 31 of the 41 DOLPHIN models proved to be very selective toward their type-II ligands with the AUC exceeding 0.9. As expected, poor selectivity was observed for the imatinib-resistant mutant structures of ABL1 (2z60A and 2v7aA,B), the three salt-bridge-deficient SRC structures (1fmkA, 2hwoA, and 1yomB), and the high B-factor ABL1 structure (2hz4C). Notably, the models that performed best in docking (e.g., 2g2iA, 2qohA,B and 1oz1A) also demonstrated the highest screening selectivity.

Clearly, the quality of the source X-ray structures may have a dramatic effect on the results of DOLPHIN docking and screening. This quality, however, is not exhausted by simple characteristics such as the average resolution of the structure or even atomic B-factor values. For example, the 3.12 Å resolution structure 2g2iA of ABL1 (maximal pocket B-factor of 147) and the 2.9 Å resolution structures 2fb8A,B of BRAF1 nevertheless demonstrated very high docking and screening performance. Conversely, high-resolution, low B-factors, or even good electron density in the vicinity of the binding pocket can sometimes be observed in a poorly performing model. For example, the excellently resolved SRC structure, 1fmkA (reso-

Table 2. VLS Performance of Individual DOLPHIN Models Evaluated as the Area under Their ROC Curves[a]

ABL1	AUC
2qohA	0.95
2qohB	0.95
2g2iA	0.95
2g2iB	0.94
2f4jA	0.93
2hz4B	0.91
2gqgB	0.91
2hz4A	0.89
2z60A[c]	0.88
2gqgA[b]	0.83
2v7aA[c]	0.81
2hz4C	0.73
2v7aB[c]	0.66
KIT	**AUC**
1pkgB[b]	0.96
1pkgA[b]	0.92
MK14	**AUC**
1oz1A	0.97
1oukA	0.97
1ouyA	0.95
1m7qA	0.95
2okrD	0.94
2okrA	0.93
BRAF1	**AUC**
2fb8B	0.98
2fb8A	0.97
LCK	**AUC**
2ofuA	0.97
3lckA	0.97
1qpcA	0.96
1qpeA	0.96
2of2A	0.95
2of4A	0.95
1qpjA	0.92
1qpdA	0.92
SRC	**AUC**
2oiqB[b]	0.96
2bdjA[b]	0.96
1yi6B[b]	0.94
1y57A	0.93
2bdfB[b]	0.91
2bdfA[b]	0.90
1yi6A	0.82
1fmkA[d]	0.77
2hwoA[e]	0.73
1yomB[e]	0.50

[a] Three to fourteen active type-II compounds per kinase were recognized in a set of 391 kinase ligands. [b] Narrow pocket. [c] T315I imatinib-resistant mutation. [d] Conserved salt bridge disrupted. [e] Conserved salt bridge disordered.

lution 1.5 Å, pocket atom B-factors not exceeding 54), appeared to be type-II incompatible because of a disrupted salt bridge. Whereas it has been previously shown that large-scale virtual screening efforts provide better results for high-resolution structures, in DOLPHIN docking and screening, the influence of structure quality is watered down by other factors. For this study, we used structures with resolutions below 3.5 Å. Where available, local pocket electron density was checked by the use of the Uppsala electron density server[30] and was found to be acceptable in all cases.

Virtual Ligand Screening with Multiple Models of the Same Kinase. The ligand hit lists from all DOLPHIN models of a single kinase were combined, with each compound represented by its best score in the ensemble. This approach provided exceptionally high selectivity for all six kinases, with AUC values of 0.96, 0.97, 0.95, 0.96, 0.98, and 0.96 for ABL1, BRAF1, KIT, LCK, MK14, and SRC, respectively (Figure 5).

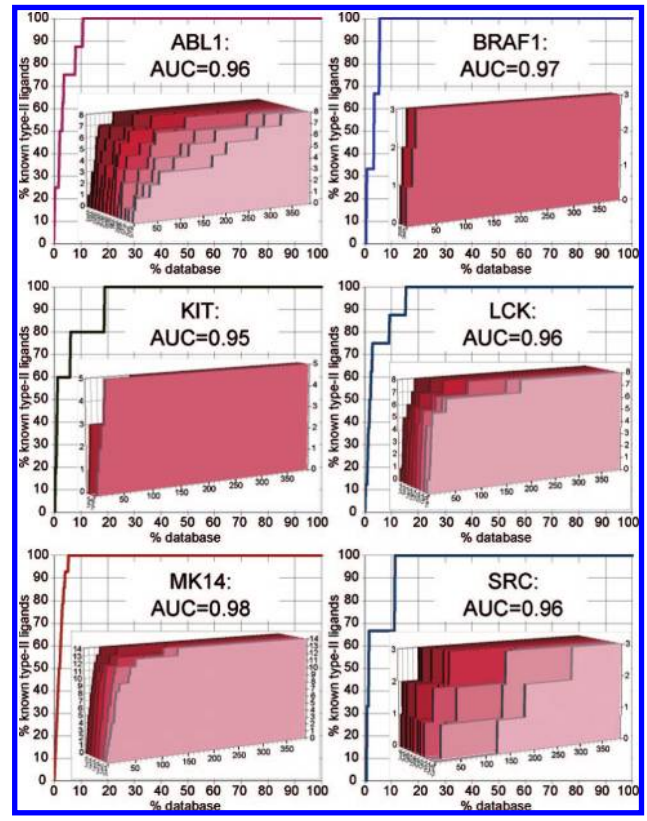

Figure 5. VLS performance of DOLPHIN MRC ensembles, evaluated as the area under their ROC curves. Three to fourteen active type-II compounds per kinase were recognized in a set of 391 kinase ligands. Red 3D inserts represent the ROC curves for individual DOLPHINs.

Most (>50%) of the known type-II ligands were ranked in the top 3.32% of the list for ABL1 and BRAF1 and in the top 1.28, 2.56, 2.30 and 1.79% for KIT, LCK, MK14, and SRC, respectively. Even the narrow-pocket KIT ensemble recognized three of five type-II inhibitors of KIT (compounds **3**, **4**, and **5**, Figure 3) as ranks two, four, and five, respectively.

Application of the DOLPHIN Screening: Identification of Compound Off-Target Activities. We further analyzed the top ~5% of each hit list by looking specifically at the hypothetical false positives, that is, high-scoring compounds with no reported activity against the respective kinases. This exercise resulted in the identification of the following secondary activities of crystallographic type-II inhibitors (Figure 6): (1) Compound **6**, a dual TIE2 and VGFR2 tyrosine kinase inhibitor[10] (PDB Het ID GIG), scored well in the DOLPHIN ensembles of SRC and MK14 kinases (ranks 3 and 18 of 391, respectively). Its inhibitory activity against these kinases was experimentally confirmed (Masaichi Hasegawa, personal communication). (2) Compound **7** (INNO-406), a potent inhibitor of ABL1 and Lyn kinases[31] (PDB Het ID 406), was among the top-scoring compounds in the LCK ensemble (rank 33 of 391). That prediction was also confirmed because INNO-406 inhibits LCK with $IC_{50} \approx 120$ nM.[32] (3) Compound **8**, a VGFR2 inhibitor[33] (PDB Het ID 276), ranked fourth in the DOLPHIN ensemble of BRAF1. It was also confirmed to inhibit this kinase with $IC_{50} \approx 400$ nM (Michele Potashman, personal communication).

Identification of a Potent and Selective Inhibitor of CSK Kinase. Our approach was further applied to a kinase with no available DFG-out structure. We chose human C-terminal Src kinase, CSK, for this case study because it had a DFG-in

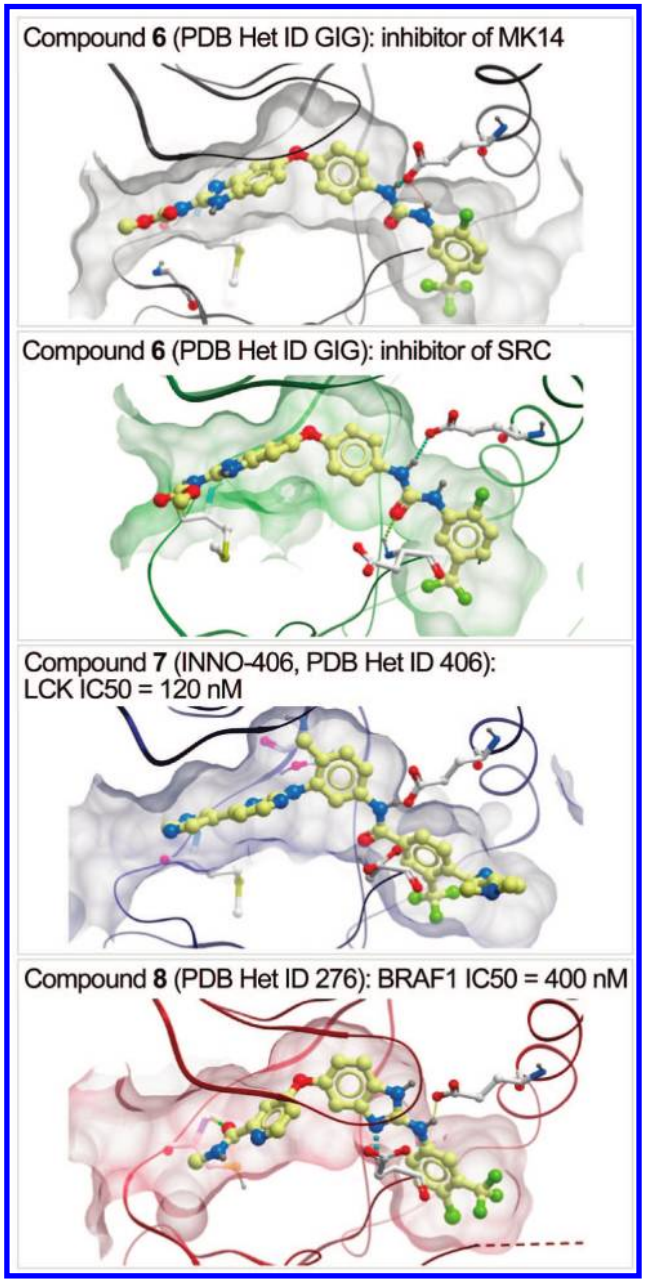

Figure 6. Examples of compound secondary activity prediction using DOLPHIN screening. Top-scoring poses of the inhibitors in DOLPHIN models of the off-target kinases are shown. The inhibition of these kinases was confirmed by the authors of the original studies.

structure in the public domain (PDB 1k9a[34]) and a known type-II inhibitor.[20] We built the DOLPHIN models from all six chains of the structure and screened all second-generation type-II inhibitors[20] against the obtained MRC ensemble. Compound **9**, the only annotated type-II CSK inhibitor in the set,[20] ranked first in the resulting hit list.

Protein-Specific Binding Energy Offsets and In Silico Compound Profiling. Computational prediction of the relative binding affinity of a compound for different proteins remains an unsolved problem despite the significant progress toward better force fields and scoring functions. A major difficulty is presented by the fact that binding energies estimated from protein−ligand complex structures appear to be shifted from the observed binding energies in a systematic, protein-specific fashion. Apart from inevitable fluctuations in model quality and energy functions, these systematic binding energy offsets are caused by thermodynamic reasons, namely, variations of the protein conformational equilibrium.

The latter considerations are of particular importance to the present study. Our ligands of interest bind exclusively to the DFG-out kinase species, so their observed affinity depends on the relative concentrations of DFG-in and DFG-out molecules. Equilibrium variations between kinases, mutants of the same kinase, and experimental conditions introduce different offsets to the observed binding energies. For example, experimental data analysis gives the estimated offset difference of 3.15 kcal/mol to the observed type-II compound binding energy to phosphorylated versus unphosphorylated ABL1, 0.7 kcal/mol to LCK versus ABL1, and 4 kcal/mol to SRC versus ABL1. (See the Supporting Information.) Here we demonstrate that the addition of the offsets to the binding energy estimates from DOLPHIN complexes makes them suitable for ligand activity profiling.

Computational Determination of Kinase-Specific Binding Energy Offsets. For most kinases, the offsets cannot be directly derived from experimental data and must be found by fitting experimental to calculated binding energies. Using this approach, we obtained the following offset differences for the five kinases with respect to unphosphorylated ABL1: $b_{BRAF1} - b_{ABL1} = 1.17$ kcal/mol, $b_{KIT} - b_{ABL1} = -4.48$ kcal/mol, $b_{LCK} - b_{ABL1} = 0.20$ kcal/mol, $b_{MK14} - b_{ABL1} = -0.17$ kcal/mol, and $b_{SRC} - b_{ABL1} = 3.55$ kcal/mol.

For the two kinases whose relative offsets with respect to ABL1 could be estimated from the experimental binding data (LCK and SRC), these values are in good agreement with the experiment (0.20 vs 0.7 kcal/mol for LCK and 3.55 vs 4 kcal/mol for SRC). The unusually low predicted offset for KIT (−4.48 kcal/mol) is due to the properties of the source DFG-in structures rather than the equilibrium considerations; the calculated binding energies for the correctly docked ligands were consistently higher in the narrow pocket KIT ensemble than in other kinases.

Type-II Ligand Activity/Selectivity Profiling with DOLPHIN Models. The kinase-specific binding energy offsets were combined with previously calculated ligand binding scores in the DOLPHIN MRC ensembles to give the estimates of their observed binding affinities. The comparison of the obtained values with the experimental data showed a strong correlation (Figure 7). For example, the DOLPHIN models correctly characterized compound imatinib (PDB Het ID STI) as a potent inhibitor of ABL1 and LCK kinases but not of BRAF1, MK14, or SRC. BIRB-796 (PDB Het ID B96) was found to be more active against MK14 than against the other five kinases. Sorafenib (PDB Het ID BAX) was confirmed to be a relatively nonspecific compound that inhibits all six kinases, SRC to a lesser extent than others. The plot features only two false negatives: INNO-406 and imatinib were not identified as the inhibitors of KIT because of their poor scoring in the available KIT DFG-in structures.

Several false positives on the plot are likely due to the mixed nature of the experimental data: our calculated binding affinities approximated K_d but were fitted to mixed $IC_{50}/K_d/K_i$ data. The experimental IC_{50}/K_d ratios are known to vary from 1 to >100 because of unnatural peptide substrates, a dependence on the ATP concentration relative to the $K_{M,ATP}$, and other factors,[35,36] which most likely explains the observed deviations.

Discussion

Recent advances in medicinal chemistry demonstrated that the type-II inhibition phenomenon might extend to a wide range

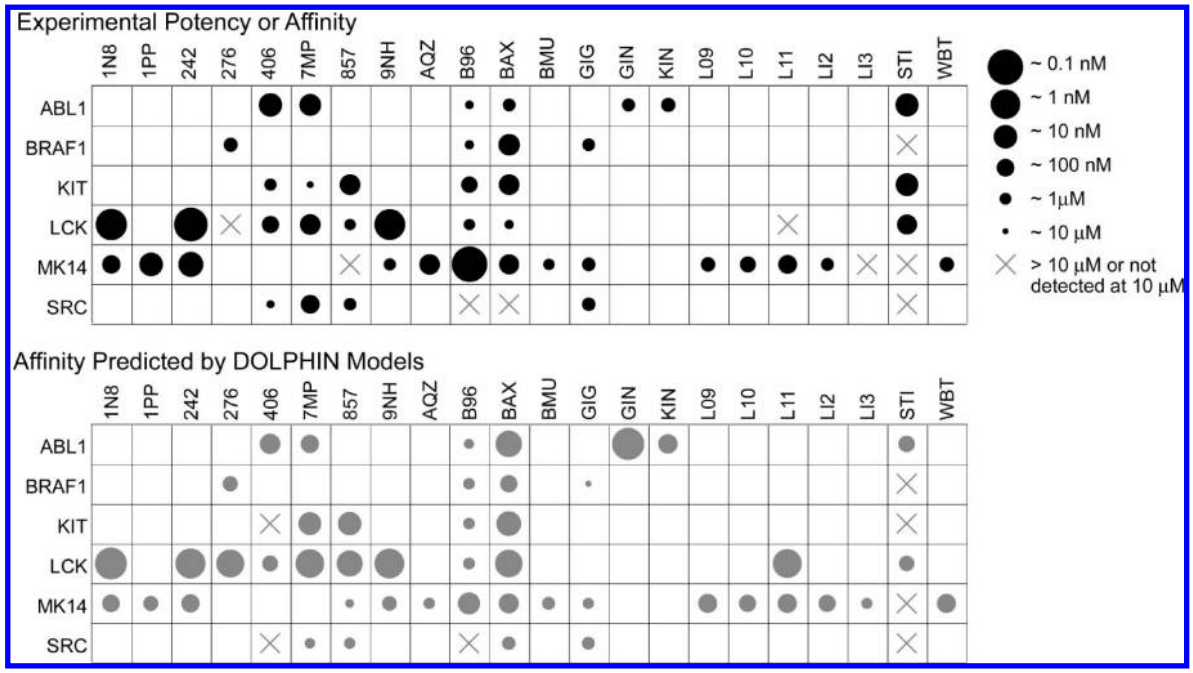

Figure 7. Comparison of experimental activities of known type-II kinase inhibitors with their binding affinities predicted by the DOLPHIN kinase models.

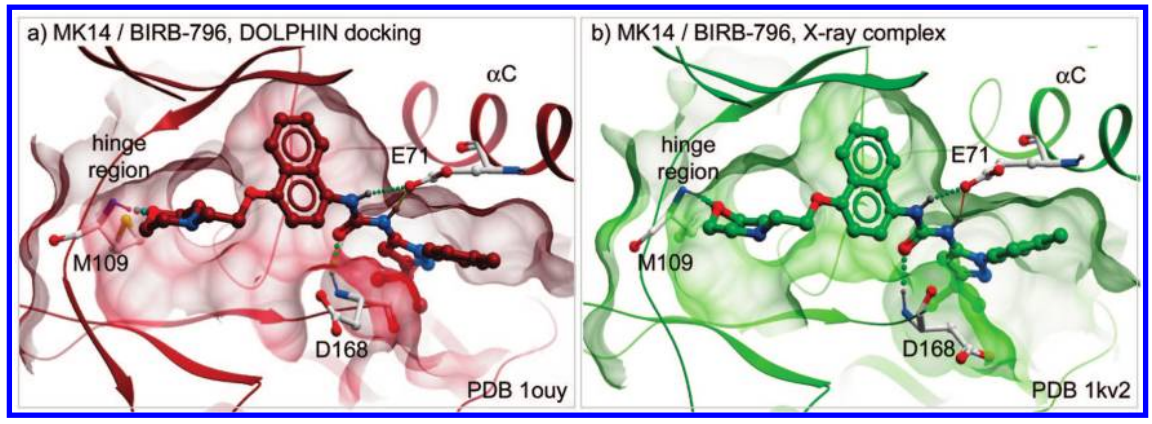

Figure 8. Side-by-side comparison of (a) the best scoring pose of compound **10** (BIRB-796) in the DOLPHIN ensemble of the MK14 kinase with (b) the crystallographic complex. DOLPHIN docking reproduces the detailed interatomic contacts. Hydrogen bonds are shown as colored dots; the receptor pocket surface is shown as transparent mesh.

of kinases[10,12] and ligand chemotypes (e.g., refs 33 and 37). Unfortunately, the efficient structure-based discovery of type-II inhibitors is hindered by the lack of compatible kinase structures. The better stability of the DFG-in state makes it a primary material for both experimental ligand screening and X-ray crystallography, introducing a strong bias toward DFG-in conformations in the structural kinome. We demonstrated that despite their obvious type-II incompatibility, the DFG-in structures often preserve the determinants of type-II ligand binding and can be converted to accurate and specific models of type-II-bound kinases.

Building and testing the DOLPHIN models on a comprehensive kinase benchmark revealed their potential for predicting type-II ligand binding poses (95% success). The top-ranking ligand poses also reproduced the detailed interatomic contacts of the complex. Figure 8 provides a comparison of DOLPHIN docking and crystallographic complexes of compound **10** (BIRB-796) with MK14 kinase; the predicted complex reconstitutes all essential intermolecular hydrogen bonds and nonpolar contacts identified by X-ray crystallography.[9] Similar results were achieved with other ligand/kinase pairs. The accurate prediction of interatomic contacts makes DOLPHIN docking complexes good starting points for structure-based ligand optimization.

Most DOLPHIN models demonstrated high screening selectivity, even as single rigid receptors. By taking into account the kinase conformational flexibility (MRC approach) we further improved the results, providing recognition of most known type-II inhibitors in the top 1.5−3.5% of the hit lists. We therefore recommend DOLPHIN MRC ensembles as the most efficient virtual screening tool. We were especially pleased to observe that several cases that were initially classified as false positives were later confirmed as secondary (off-target) activities of the benchmark compounds. This validated the use of the DOLPHIN approach for compound off-target activity prediction, a task of critical practical importance.

The DOLPHIN protocol proved to be sensitive to kinase active site mutations. The three ABL1 structures carrying a T315I imatinib-resistance mutation (2v7aA,B and 2z60A) clearly behaved differently in docking and screening, down-scoring the inhibitors of the wild-type kinase. Instead, high scores and ranks

were assigned to different compounds that now await experimental validation as type-II inhibitors of T315I ABL1.

The current established understanding of the phenomenon of type-II inhibition gives two major reasons for higher affinity (or exclusive binding) of a type-II inhibitor for one of two different kinases. The first and most obvious reason lies in variations of the binding site residue composition. (It explains, for example, why imatinib binds to ABL1 but not to MK14.) In particular, a single change in the gatekeeper residue may exhibit the most profound effect on the inhibitor binding because of a steric clash. Another more subtle reason is the varying energetic penalty of adopting the DFG-out conformation. (This, for example, explains the low observed affinity of imatinib for SRC.[28]) The two reasons, though not entirely independent,[38] do not appear to correlate directly across the kinome; a small gatekeeper does not result in high DFG-out propensity (e.g., SRC has a small gatekeeper and low DFG-out propensity) and vice versa (e.g., IGF1R has a bulky gatekeeper but high DFG-out propensity). Whereas the calculated binding energies for DOLPHIN docking complexes capture the residue composition aspect of the binding affinity, the predefined kinase-specific systematic binding energy offsets introduced in this study represent the numerical expression of the DFG-out propensities. By combining these values, we showed that the DOLPHIN approach could be used to predict the affinity of a single inhibitor for different kinases, to evaluate its cross reactivity, and to determine its selectivity profile. That puts our computational technique in line with advanced in vitro activity profiling assays,[39] addressing a particularly challenging problem of targeting inactive kinase conformations.

High selectivity may or may not be a desirable feature for a kinase inhibitor. In recent years, several compounds annotated as multi-targeted kinase inhibitors entered clinical trials and were proved to exhibit therapeutic effects by simultaneously shutting down more than one kinase in the same or related pathways. The rational development of such compounds requires both extensive screening and profiling. Combined with experimentally derived protein-specific offsets, the methodology proposed in this article may be of great help in the design of inhibitors with desired activity profiles.

Ab initio prediction of the absolute DFG-out propensity values and related binding energy offsets for different kinases is an unsolved problem and is out of the scope of this paper. However, the propensity can be deduced from experimental binding data on at least one known type-II inhibitor. Recent large-scale kinase inhibitor profiling efforts (e.g., refs 39 and 40) provide data for the indirect evaluation of the fraction of kinases with significant DFG-out propensity and for estimating selected kinase-specific offsets. For example, at least 108 of 281 protein kinases tested by Ambit[39] (mutants excluded) bind five known type-II inhibitors, **1** (imatinib[6]), **3** (sorafenib,[41]), **10** (BIRB-796[9]), **11** (ABT-869[42]), and **12** (AST-487[43,44]), with an affinity of ≤ 1 μM. A similar tendency is observed within the Ser/Thr kinase domain extensively screened by Fedorov et al.[40] It is very unlikely that the inhibitors achieve this high potency while binding the kinases in DFG-in conformations; therefore, 40% (i.e., 108/281) represents a reasonable estimate of the fraction of kinases readily adopting a DFG-out conformation in solution. Interestingly, 44 of the 108 kinases have crystal structures in PDB; among them, only 8 are crystallized with a type-II inhibitor, but 26 (60%) are found in the classical DFG-in conformation thus representing immediate candidates for DOLPHIN transformation and DOLPHIN-based compound cross-reactivity studies.

In summary, the proposed DOLPHIN methodology provides reliable structure-based identification of novel type-II ligands, their binding geometries, and their kinase selectivity profiles. The abundance of DFG-in conformations in the structural kinome makes this approach applicable to a wide range of kinases, opening new possibilities for the discovery of novel specific kinase-targeting therapeutics in cancer and other diseases.

Methods

Identification of Protein Kinase Domains. Protein kinase domain sequence annotations were taken from SwissProt[45,46] (release 55.5 of June 2008). The sequences were searched against a nonredundant subset of PDB sequences with common protein tags removed. The identified kinase domain structures were clustered to 95% sequence identity. The procedure yielded 122 mammalian kinases with available X-ray 3D information (856 PDB entries, 1216 structures when distinct chains within a single PDB entry are separately counted).

Automated Conformational Classification of the Entire Structural Kinome. Each kinase domain was superimposed onto a template DFG-in structure of ABL1 kinase (PDB ID 2gqg, chain A) using only backbone heavy atoms in the 5A vicinity of the imatinib binding site with the activation loop excluded. Residue matching for the superimposition was established from a sequence alignment. The superimposition algorithm iteratively optimized a weighted rmsd with lower weights assigned to the minority of the most deviating atoms.

DFG-in/DFG-out classification of the superimposed structure was performed on the basis of the position and the orientation of the middle residue in its DFG motif. The orientation of the residue was determined as the sum of cosines of angles between the four covalent bonds formed by its C_α, C_β, C_γ, and $C_\delta{}^{1,2}$ atoms and the corresponding bonds in the template structure. The resulting Phe orientation index, O_{phe}, ranged from 0 to 4, with larger values indicating similar orientations. The position of the residue, P_{phe}, was defined as the distance between its C_α atom and the Phe382 C_α of the template structure. The so-called DFG-in score ($S_{\text{DFG-in}}$) was calculated for each kinase domain as follows

$$S_{\text{DFG-in}} = \sqrt{P_{\text{phe}}^2 + 2(O_{\text{phe}} - 4)^2}$$

Figure S3 in the Supporting Information presents the histogram of distribution of DFG-in scores for all X-ray structures of kinase domain in PDB and examples of structures with different values of the DFG-in score.

For the purpose of this study, a kinase domain structure was classified as DFG-in if its DFG-in score was below three. It was classified as DFG-out if no more than one heavy atom was present in the 2 Å vicinity of the DFG phenyl ring of the template structure after superimposition. The structures in which the DFG motif was disordered or overlapped with the template DFG with $S_{\text{DFG-in}} \geq 3$ were considered to be intermediate (neither DFG-in nor DFG-out).

A small molecule ligand was classified as a type-II ligand if it had more than four atoms in the 2 Å vicinity of the DFG phenyl ring of the template after kinase domain superimposition. The corresponding kinase domain structure was called a type-II-bound structure.

Benchmark for Ligand Binding Geometry Prediction by DOLPHIN Models. The DOLPHIN docking set consisted of all kinases for which both DFG-in and type-II-bound X-ray structures were found in the PDB release of March 2008. It included 41 DFG-in structures of 6 kinases and 20 crystallographic type-II inhibitors (Table 1, Table S2 in the Supporting Information). Each ligand was found in a cocrystal with one kinase, except imatinib cocrystallized with ABL1, SRC, KIT, and LCK. This produced a total of 23 kinase/inhibitor pairs and 184 DFG-in structure/inhibitor docking pairs.

Benchmark for Testing DOLPHIN Model Screening and Selectivity Properties. A comprehensive set of crystallographic kinase inhibitors was collected from the PDB release of March 2008

(391 compounds). Among them, 28 compounds (Table S1 and Figures S1 and S2 in the Supporting Information) have been cocrystallized in the type-II binding mode with one or more kinase. Each of these compounds was classified as a binder to a kinase if it had been found in a cocrystal with that kinase in the PDB or if one of the experimentally determined IC_{50}, K_i, or K_d values was below 10 μM; otherwise, it was considered to be a nonbinder. The type-II binders made the positive part of the set for the kinase; all other compounds, including ATP-site inhibitors and type-II ligands with no available activity data, were considered to be negative. The positive parts of the set for ABL1, BRAF1, KIT, LCK, MK14, and SRC consisted of 8, 3, 5, 8, 14, and 3 type-II compounds, respectively.

DOLPHIN Model Preparation from DFG-In Kinase Structures. The DOLPHIN model preparation protocol consisted of two fully automatic steps: (i) the removal of all atoms of DFG Phe and the next four residues in the sequence and (ii) the generation of the pharmacophore-like field from side-chain atoms of DFG Phe and backbone atoms of the following residues with DFG Gly skipped (Figures 2a, 2b). The pharmacophore-like density was generated in the spirit of atomic property fields[47] using a single property (lipophilicity). The density slightly rewarded the ligand docking poses occupying the hydrophobic selectivity pocket. No ligand-related information was employed by the algorithm.

Internal Coordinate Mechanics Grid Docking. ICM molecular modeling software[48,49] was used for ligand docking and scoring. ICM ligand docking is based on biased probability Monte Carlo optimization of the ligand internal coordinates in the set of grid potential maps of the receptor. A diverse set of conformers was first generated from PDB ligand coordinates by ligand sampling in vacuo. Each conformer was locally minimized with relaxed bond lengths and bond angles by the use of the MMFF-94 force field to remove any bias toward receptor-bound covalent geometry. The generated conformers were then placed in the binding pocket in four principal orientations and were used as starting points for Monte Carlo optimization. The optimized energy function included the ligand internal strain and a weighted sum of the grid map values in ligand atom centers. The attractive DOLPHIN density map was added to the standard set of ICM receptor maps. The number of sampling steps was limited to 50 000 per ligand per receptor (20−40 s on Intel Core 2 Duo E6600 at 2.40 GHz).

Internal Coordinate Mechanics Full-Atom Ligand−Receptor Complex Refinement and Scoring. The top-scoring ligand poses were merged with their DOLPHIN receptors to obtain full-atom models of the complexes. Each complex was refined by local gradient minimization of the ligand and surrounding pocket side chains and global Monte Carlo optimization of rotatable hydrogens. During the refinement, the ligand heavy atoms were tethered to their docking positions with a harmonic restraint whose weight was iteratively decreased.

The complexes were evaluated with a full-atom ICM ligand binding score[26] that has been previously derived from a multireceptor screening benchmark as a compromise between approximated Gibbs free energy of binding and numerical errors. The score was calculated by:

$$S_{bind} = E_{int} + T\Delta S_{Tor} + E_{vw} + \alpha_1 E_{el} + \alpha_2 E_{hb} + \alpha_3 E_{hp} + \alpha_4 E_{sf}$$

where E_{vw}, E_{el}, E_{hb}, E_{hp}, and E_{sf} are van der Waals, electrostatic, hydrogen bonding, and nonpolar and polar atom solvation energy differences between bound and unbound states, respectively. E_{int} is the ligand internal strain, ΔS_{Tor} is its conformational entropy loss upon binding, and $T = 300$ K, and α_i are ligand- and receptor-independent constants. The score was artificially increased for irrelevant ligand poses outside the hydrophobic/selectivity pocket, that is, more than 2 Å from the side chain of the removed DFG Phe or more than 5 Å from the C_β atom of either conserved Lys or the gatekeeper.

Virtual Ligand Screening. The 391 crystallographic kinase ligands were docked in each DOLPHIN model. The top three poses per ligand were refined and rescored. An ordered ligand hit list was built from the best scoring ligand poses. The ROC-curves were obtained by plotting the number of top compounds in the list against the number of correct type-II ligands among them.

Determination of Kinase-Specific Binding Energy Offsets and Compound Profiling. The observed Gibbs energy of binding of a ligand to a kinase, ΔG_b^{obs}, was calculated to be $RT \ln k$, $T = 300$ K. Where available, we used the binding constant K_d for k; in all other cases, IC_{50} or K_i values were used. We assumed a linear relation between the experimental ΔG_b^{obs} and the calculated binding score

$$G_b^{obs} = mS_{bind} + b$$

where m is a universal constant and b is a kinase-dependent binding energy offset. The set of 53 kinase−inhibitor pairs with available experimental binding data was described by a vector S_{bind} of the calculated binding scores and six kinase characterization vectors, σ_j ($j \in$ {ABL1, BRAF1, KIT, LCK, MK14, SRC}, $\sigma_j = 1$ for all data points with j as the target kinase, 0 for the rest). Partial least squares regression was trained to predict experimental ΔG_b^{obs} as a function of S_{bind} and σ_j

$$\Delta G_b^{obs} = mS_{bind} + \sum b_j \sigma_j$$

The obtained values of b_j gave the kinase-specific binding energy offsets. They were used to predict the binding energy for each kinase−inhibitor pair to be $\Delta G_b^{pred} = mS_{bind} + b_j$, where b_j is the offset for the corresponding kinase.

Acknowledgment. We thank Ketan S. Gajiwala of Pfizer, and Mazen W. Karaman of Ambit, for valuable discussions. We also thank Michelle Potashman of Amgen, Tomoko Niwa of Nippon Shinyaku, and Masaichi Hasegawa of GlaxoSmith-Kline for providing activity data on PDB Het IDs 276, 406, and GIG, respectively. All molecular images were prepared using ICM (http://www.molsoft.com/icm/). This work was supported by NIH grant 1-R01-GM074832-01A1.

Supporting Information Available: Compound structures and experimental activities, DFG-in score distribution in the publicly available structural kinome, benchmark for DOLPHIN ligand binding geometry prediction, and derivation of kinase-specific binding energy offsets. This material is available free of charge via the Internet at http://pubs.acs.org.

References

(1) Manning, G.; Whyte, D. B.; Martinez, R.; Hunter, T.; Sudarsanam, S. The Protein Kinase Complement of the Human Genome. *Science* **2002**, *298*, 1912–1934.
(2) Cohen, P. Protein Kinases: The Major Drug Targets of the Twenty-First Century. *Nat. Rev. Drug Discovery* **2002**, *1*, 309–315.
(3) Bogoyevitch, M. A.; Fairlie, D. P. A New Paradigm for Protein Kinase Inhibition: Blocking Phosphorylation without Directly Targeting ATP Binding. *Drug Discovery Today* **2007**, *12*, 622633..
(4) Schindler, T.; Bornmann, W.; Pellicena, P.; Miller, W. T.; Clarkson, B.; Kuriyan, J. Structural Mechanism for STI-571 Inhibition of Abelson Tyrosine Kinase. *Science* **2000**, *289*, 1938–1942.
(5) Lowinger, T. B.; Riedl, B.; Dumas, J.; Smith, R. A. Design and Discovery of Small Molecules Targeting Raf-1 Kinase. *Curr. Pharm. Des.* **2002**, *8*, 2269–78.
(6) Cowan-Jacob, S. W.; Fendrich, G.; Floersheimer, A.; Furet, P.; Liebetanz, J.; Rummel, G.; Rheinberger, P.; Centeleghe, M.; Fabbro, D.; Manley, P. W. Structural Biology Contributions to the Discovery of Drugs to Treat Chronic Myelogenous Leukaemia. *Acta Crystallogr., Sect. D: Biol. Crystallogr.* **2007**, *63*, 80–93.
(7) Nagar, B.; Bornmann, W. G.; Pellicena, P.; Schindler, T.; Veach, D. R.; Miller, W. T.; Clarkson, B.; Kuriyan, J. Crystal Structures of the Kinase Domain of c-Abl in Complex with the Small Molecule Inhibitors PD173955 and Imatinib (STI-571). *Cancer Res.* **2002**, *62*, 4236–4243.
(8) Weisberg, E.; Manley, P. W.; Breitenstein, W.; Brüggen, J.; Cowan-Jacob, S. W.; Ray, A.; Huntly, B.; Fabbro, D.; Fendrich, G.; Hall-Meyers, E.; Kung, A. L.; Mestan, J.; Daley, G. Q.; Callahan, L.;

Catley, L.; Cavazza, C.; Mohammed, A.; Neuberg, D.; Wright, R. D.; Gilliland, D. G.; Griffin, J. D. Characterization of AMN107, a selective inhibitor of native and mutant Bcr-Abl. *Cancer Cell* **2005**, *7*, 129–141.

(9) Pargellis, C.; Tong, L.; Churchill, L.; Cirillo, P. F.; Gilmore, T.; Graham, A. G.; Grob, P. M.; Hickey, E. R.; Moss, N.; Pav, S.; Regan, J. Inhibition of p38 MAP Kinase by Utilizing a Novel Allosteric Binding Site. *Nat. Struct. Mol. Biol.* **2002**, *9*, 268–272.

(10) Hasegawa, M.; Nishigaki, N.; Washio, Y.; Kano, K.; Harris, P. A.; Sato, H.; Mori, I.; West, R. I.; Shibahara, M.; Toyoda, H.; Wang, L.; Nolte, R. T.; Veal, J. M.; Cheung, M. Discovery of Novel Benzimidazoles as Potent Inhibitors of TIE-2 and VEGFR-2 Tyrosine Kinase Receptors. *J. Med. Chem.* **2007**, *50*, 4453–4470.

(11) Hodous, B. L.; Geuns-Meyer, S. D.; Hughes, P. E.; Albrecht, B. K.; Bellon, S.; Caenepeel, S.; Cee, V. J.; Chaffee, S. C.; Emery, M.; Fretland, J.; Gallant, P.; Gu, Y.; Johnson, R. E.; Kim, J. L.; Long, A. M.; Morrison, M.; Olivieri, P. R.; Patel, V. F.; Polverino, A.; Rose, P.; Wang, L.; Zhao, H. Synthesis, Structural Analysis, and SAR Studies of Triazine Derivatives as Potent, Selective Tie-2 Inhibitors. *Bioorg. Med. Chem. Lett.* **2007**, *17*, 2886–2889.

(12) Cai, Z.-W.; Wei, D.; Schroeder, G. M.; Cornelius, L. A. M.; Kim, K.; Chen, X.-T.; Schmidt, R. J.; Williams, D. K.; Tokarski, J. S.; An, Y.; Sack, J. S.; Manne, V.; Kamath, A.; Zhang, Y.; Marathe, P.; Hunt, J. T.; Lombardo, L. J.; Fargnoli, J.; Borzilleri, R. M. Discovery of Orally Active Pyrrolopyridine- and Aminopyridine-Based Met kinase Inhibitors. *Bioorg. Med. Chem. Lett.* **2008**, *18*, 3224–3229.

(13) Fabian, M. A.; Biggs, W. H.; Treiber, D. K.; Atteridge, C. E.; Azimioara, M. D.; Benedetti, M. G.; Carter, T. A.; Ciceri, P.; Edeen, P. T.; Floyd, M.; Ford, J. M.; Galvin, M.; Gerlach, J. L.; Grotzfeld, R. M.; Herrgard, S.; Insko, D. E.; Insko, M. A.; Lai, A. G.; Lelias, J.-M.; Mehta, S. A.; Milanov, Z. V.; Velasco, A. M.; Wodicka, L. M.; Patel, H. K.; Zarrinkar, P. P.; Lockhart, D. J. A Small Molecule−Kinase Interaction Map for Clinical Kinase Inhibitors. *Nat. Biotechnol.* **2005**, *23*, 329–336.

(14) Nordin, H.; Jungnelius, M.; Karlsson, R.; Karlsson, O. P. Kinetic Studies of Small Molecule Interactions with Protein Kinases Using Biosensor Technology. *Anal. Biochem.* **2005**, *340*, 359–368.

(15) Patricelli, M. P.; Szardenings, A. K.; Liyanage, M.; Nomanbhoy, T. K.; Wu, M.; Weissig, H.; Aban, A.; Chun, D.; Tanner, S.; Kozarich, J. W. Functional Interrogation of the Kinome Using Nucleotide Acyl Phosphates. *Biochemistry* **2007**, *46*, 350–358.

(16) Bantscheff, M.; Eberhard, D.; Abraham, Y.; Bastuck, S.; Boesche, M.; Hobson, S.; Mathieson, T.; Perrin, J.; Raida, M.; Rau, C.; Reader, V.; Sweetman, G.; Bauer, A.; Bouwmeester, T.; Hopf, C.; Kruse, U.; Neubauer, G.; Ramsden, N.; Rick, J.; Kuster, B.; Drewes, G. Quantitative Chemical Proteomics Reveals Mechanisms of Action of Clinical ABL Kinase Inhibitors. *Nat. Biotechnol.* **2007**, *25*, 1035–1044.

(17) Mayhood, T. W.; Windsor, W. T. Ligand Binding Affinity Determined by Temperature-Dependent Circular Dichroism: Cyclin-Dependent Kinase 2 Inhibitors. *Anal. Biochem.* **2005**, *345*, 187–197.

(18) Vedadi, M.; Niesen, F. H.; Allali-Hassani, A.; Fedorov, O. Y.; Finerty, P. J.; Wasney, G. A.; Yeung, R.; Arrowsmith, C.; Ball, L. J.; Berglund, H.; Hui, R.; Marsden, B. D.; Nordlund, P.; Sundstrom, M.; Weigelt, J.; Edwards, A. M. Chemical Screening Methods to Identify Ligands That Promote Protein Stability, Protein Crystallization, and Structure Determination. *Proc. Natl. Acad. Sci. U.S.A.* **2006**, *103*, 15835–15840.

(19) Thompson, P. A.; Wang, S.; Howett, L. J.; Wang, M.-M.; Patel, R.; Averill, A.; Showalter, R. E.; Li, B.; Appleman, J. R. Identification of Ligand Binding by Protein Stabilization: Comparison of ATLAS with Biophysical and Enzymatic Methods. *Assay Drug. Dev. Technol.* **2008**, *6*, 69–81.

(20) Liu, Y.; Gray, N. S. Rational Design of Inhibitors That Bind to Inactive Kinase Conformations. *Nat. Chem. Biol.* **2006**, *2*, 358–364.

(21) Okram, B.; Nagle, A.; Adrian, F. J.; Lee, C.; Ren, P.; Wang, X.; Sim, T.; Xie, Y.; Wang, X.; Xia, G.; Spraggon, G.; Warmuth, M.; Liu, Y.; Gray, N. S. A General Strategy for Creating "Inactive-Conformation" Abl Inhibitors. *Chem. Biol.* **2006**, *13*, 779–786.

(22) Totrov, M.; Abagyan, R. Flexible Protein−Ligand Docking by Global Energy Optimization in Internal Coordinates. *Proteins: Struct., Funct., Genet.* **1997**, *29*, 215–220.

(23) Chen, H.; Lyne, P. D.; Giordanetto, F.; Lovell, T.; Li, J. On Evaluating Molecular-Docking Methods for Pose Prediction and Enrichment Factors. *J. Chem. Inf. Model.* **2006**, *46*, 401–415.

(24) Lovell, T.; Chen, H.; Lyne, P. D.; Giordanetto, F.; Li, J. On Evaluating Molecular-Docking Methods for Pose Prediction and Enrichment Factors. [*J. Chem. Inf. Model*. *46*, 401−415 (2006)]. *J. Chem. Inf. Model.* **2008**, *48*, 246.

(25) Moitessier, N.; Englebienne, P.; Lee, D.; Lawandi, J.; Corbeil, C. R. Towards the Development of Universal, Fast, And Highly Accurate Docking//Scoring Methods: A Long Way to Go. *Br. J. Pharmacol.* **2007**, *153*, S7−S26.

(26) Schapira, M.; Totrov, M.; Abagyan, R. Prediction of the Binding Energy for Small Molecules, Peptides, and Proteins. *J. Mol. Recognit.* **1999**, *12*, 177–190.

(27) Berman, H. M.; Westbrook, J.; Feng, Z.; Gilliland, G.; Bhat, T. N.; Weissig, H.; Shindyalov, I. N.; Bourne, P. E. The Protein Data Bank. *Nucleic Acids Res.* **2000**, *28*, 235–242.

(28) Seeliger, M. A.; Nagar, B.; Frank, F.; Cao, X.; Henderson, M. N.; Kuriyan, J. c-Src Binds to the Cancer Drug Imatinib with an Inactive Abl/c-Kit Conformation and a Distributed Thermodynamic Penalty. *Structure* **2007**, *15*, 299–311.

(29) Sullivan, J. E.; Holdgate, G. A.; Campbell, D.; Timms, D.; Gerhardt, S.; Breed, J.; Breeze, A. L.; Bermingham, A.; Pauptit, R. A.; Norman, R. A.; Embrey, K. J.; Read, J.; VanScyoc, W. S.; Ward, W. H. J. Prevention of MKK6-Dependent Activation by Binding to p38a MAP Kinase. *Biochemistry* **2005**, *44*, 16475–16490.

(30) Kleywegt, G. J.; Harris, M. R.; Zou, J. Y.; Taylor, T. C.; Wahlby, A.; Jones, T. A. The Uppsala Electron-Density Server. *Acta Crystallogr., Sect. D: Biol. Crystallogr.* **2004**, *60*, 2240–2249.

(31) Horio, T.; Hamasaki, T.; Inoue, T.; Wakayama, T.; Itou, S.; Naito, H.; Asaki, T.; Hayase, H.; Niwa, T. Structural Factors Contributing to the Abl/Lyn Dual Inhibitory Activity of 3-Substituted Benzamide Derivatives. *Bioorg. Med. Chem. Lett.* **2007**, *17*, 2712–2717.

(32) Kimura, S.; Naito, H.; Segawa, H.; Kuroda, J.; Yuasa, T.; Sato, K.; Yokota, A.; Kamitsuji, Y.; Kawata, E.; Ashihara, E.; Nakaya, Y.; Naruoka, H.; Wakayama, T.; Nasu, K.; Asaki, T.; Niwa, T.; Hirabayashi, K.; Maekawa, T. NS-187, a Potent and Selective Dual Bcr-Abl/Lyn Tyrosine Kinase Inhibitor, is a Novel Agent for Imatinib-Resistant Leukemia. *Blood* **2005**, *106*, 3948–3954.

(33) Potashman, M. H.; Bready, J.; Coxon, A.; DeMelfi, T. M.; DiPietro, L.; Doerr, N.; Elbaum, D.; Estrada, J.; Gallant, P.; Germain, J.; Gu, Y.; Harmange, J.-C.; Kaufman, S. A.; Kendall, R.; Kim, J. L.; Kumar, G. N.; Long, A. M.; Neervannan, S.; Patel, V. F.; Polverino, A.; Rose, P.; van der Plas, S.; Whittington, D.; Zanon, R.; Zhao, H. Design, Synthesis, and Evaluation of Orally Active Benzimidazoles and Benzoxazoles as Vascular Endothelial Growth Factor-2 Receptor Tyrosine Kinase Inhibitors. *J. Med. Chem.* **2008**, *51*, 699–699.

(34) Ogawa, A.; Takayama, Y.; Sakai, H.; Chong, K. T.; Takeuchi, S.; Nakagawa, A.; Nada, S.; Okada, M.; Tsukihara, T. Structure of the Carboxyl-Terminal Src Kinase, Csk. *J. Biol. Chem.* **2002**, *277*, 14351–14354.

(35) O'Hare, T.; Druker, B. J. BIRB-796 is Not an Effective ABL(T315I) Inhibitor. *Nat. Biotechnol.* **2005**, *23*, 1209–1210.

(36) Knight, Z. A.; Shokat, K. M. Features of Selective Kinase Inhibitors. *Chem. Biol.* **2005**, *12*, 621–637.

(37) Hu, E.; Tasker, A.; White, R. D.; Kunz, R. K.; Human, J.; Chen, N.; xfc; rli, R.; Hungate, R.; Novak, P.; Itano, A.; Zhang, X.; Yu, V.; Nguyen, Y.; Tudor, Y.; Plant, M.; Flynn, S.; Xu, Y.; Meagher, K. L.; Whittington, D. A.; Ng, G. Y. Discovery of Aryl Aminoquinazoline Pyridones as Potent, Selective, and Orally Efficacious Inhibitors of Receptor Tyrosine Kinase c-Kit. *J. Med. Chem.* **2008**, *51*, 3065–3068.

(38) Azam, M.; Seeliger, M. A.; Gray, N. S.; Kuriyan, J.; Daley, G. Q. Activation of Tyrosine Kinases by Mutation of the Gatekeeper Threonine. *Nat. Struct. Mol. Biol.* **2008**, *15*, 1109–1118.

(39) Karaman, M. W.; Herrgard, S.; Treiber, D. K.; Gallant, P.; Atteridge, C. E.; Campbell, B. T.; Chan, K. W.; Ciceri, P.; Davis, M. I.; Edeen, P. T.; Faraoni, R.; Floyd, M.; Hunt, J. P.; Lockhart, D. J.; Milanov, Z. V.; Morrison, M. J.; Pallares, G.; Patel, H. K.; Pritchard, S.; Wodicka, L. M.; Zarrinkar, P. P. A Quantitative Analysis of Kinase Inhibitor Selectivity. *Nat. Biotechnol.* **2008**, *26*, 127–132.

(40) Fedorov, O.; Marsden, B.; Pogacic, V.; Rellos, P.; Muller, S.; Bullock, A. N.; Schwaller, J.; Sundstrom, M.; Knapp, S. A Systematic Interaction Map of Validated Kinase Inhibitors with Ser/Thr Kinases. *Proc. Natl. Acad. Sci. U.S.A.* **2007**, *104*, 20523–20528.

(41) Ahmad, T.; Eisen, T. Kinase Inhibition with BAY 43−9006 in Renal Cell Carcinoma. *Clin. Cancer Res.* **2004**, *10*, 6388S–6392S.

(42) Dai, Y.; Hartandi, K.; Ji, Z.; Ahmed, A. A.; Albert, D. H.; Bauch, J. L.; Bouska, J. J.; Bousquet, P. F.; Cunha, G. A.; Glaser, K. B.; Harris, C. M.; Hickman, D.; Guo, J.; Li, J.; Marcotte, P. A.; Marsh, K. C.; Moskey, M. D.; Martin, R. L.; Olson, A. M.; Osterling, D. J.; Pease, L. J.; Soni, N. B.; Stewart, K. D.; Stoll, V. S.; Tapang, P.; Reuter, D. R.; Davidsen, S. K.; Michaelides, M. R. Discovery of *N*-(4-(3-Amino-1*H*-indazol-4-yl)phenyl)-*N*′-(2-fluoro-5-methylphenyl)urea (ABT-869), a 3-Aminoindazole-Based Orally Active Multitargeted Receptor Tyrosine Kinase Inhibitor. *J. Med. Chem.* **2007**, *50*, 1584–1597.

(43) Weisberg, E.; Roesel, J.; Bold, G.; Furet, P.; Jiang, J.; Cools, J.; Wright, R. D.; Nelson, E.; Barrett, R.; Ray, A.; Moreno, D.; Hall-Meyers, E.; Stone, R.; Galinsky, I.; Fox, E.; Gilliland, G.; Daley, J. F.; Lazo-Kallanian, S.; Kung, A. L.; Griffin, J. D. Anti-Leukemic Effects of the Novel, Mutant FLT3 Inhibitor, NVP-AST487: Effects on PKC412-Sensitive and -Resistant FLT3-Expressing Cells Blood **2008**, in press.

(44) Akeno-Stuart, N.; Croyle, M.; Knauf, J. A.; Malaguarnera, R.; Vitagliano, D.; Santoro, M.; Stephan, C.; Grosios, K.; Wartmann, M.; Cozens, R.; Caravatti, G.; Fabbro, D.; Lane, H. A.; Fagin, J. A. The RET Kinase Inhibitor NVP-AST487 Blocks Growth and Calcitonin Gene Expression through Distinct Mechanisms in Medullary Thyroid Cancer Cells. *Cancer Res.* **2007**, *67*, 6956−6964.

(45) Bairoch, A.; Apweiler, R.; Wu, C. H.; Barker, W. C.; Boeckmann, B.; Ferro, S.; Gasteiger, E.; Huang, H.; Lopez, R.; Magrane, M.; Martin, M. J.; Natale, D. A.; O'Donovan, C.; Redaschi, N.; Yeh, L.-S. L. The Universal Protein Resource (UniProt). *Nucleic Acids Res.* **2005**, *33*, 154–159.

(46) Boeckmann, B.; Blatter, M.-C.; Famiglietti, L.; Hinz, U.; Lane, L.; Roechert, B.; Bairoch, A. Protein Variety and Functional Diversity: Swiss-Prot Annotation in Its Biological Context. *C.R. Biol.* **2005**, *328*, 882–899.

(47) Totrov, M. Atomic Property Fields: Generalized 3D Pharmacophoric Potential for Automated Ligand Superposition, Pharmacophore Elucidation, and 3D QSAR. *Chem. Biol. Drug Des.* **2008**, *71*, 15–27.

(48) Abagyan, R.; Totrov, M. Biased Probability Monte Carlo Conformational Searches and Electrostatic Calculations for Peptides and Proteins. *J. Mol. Biol.* **1994**, *235*, 983–1002.

(49) Abagyan, R.; Totrov, M.; Kuznetsov, D. A. ICM: A New Method for Protein Modeling and Design: Applications to Docking and Structure Prediction from the Distorted Native Conformation. *J. Comput. Chem.* **1994**, *15*, 488–506.

JM8010299